PALEOCEANOGRAPHY, VOL. 25, PA1213, doi:10.1029/2008PA001703, 2010

Atmospheric $\delta^{13}CO_2$ and its relation to pCO_2 and deep ocean $\delta^{13}C$ during the late Pleistocene

P. Köhler,[1] H. Fischer,[1,2] and J. Schmitt[1,2]

Received 16 October 2008; revised 23 October 2009; accepted 8 December 2009; published 30 March 2010.

[1] The ratio of the stable carbon isotopes of atmospheric CO_2 ($\delta^{13}CO_2$) contains valuable information on the processes which are operating on the global carbon cycle. However, current $\delta^{13}CO_2$ ice core records are still limited in both resolution and temporal coverage, as well as precision. In this study we performed simulations with the carbon cycle box model BICYCLE with special emphasis on atmospheric $\delta^{13}CO_2$, proposing how changes in $\delta^{13}CO_2$ might have evolved over the last 740,000 years. We furthermore analyze the relationship between atmospheric $\delta^{13}CO_2$, pCO_2, and deep ocean $\delta^{13}C$ of dissolved inorganic carbon (DIC) ($\delta^{13}C_{DIC}$) in both our modeling framework and proxy records (when available). Our analyses show that mean ocean and deep Pacific $\delta^{13}C_{DIC}$ are mainly controlled by the glacial/interglacial uptake and release of carbon temporarily stored in the terrestrial biosphere during warmer climate periods. In contrast glacial/interglacial changes in pCO_2 and $\delta^{13}CO_2$ represent mainly a mixture of ocean-related processes superimposed on the slow glacial/interglacial change in terrestrial carbon storage. The different processes influencing atmospheric $\delta^{13}CO_2$ largely compensate each other and cancel all variability with frequencies of 1/100 kyr^{-1}. Large excursions in $\delta^{13}CO_2$ can a priori be expected, as any small phase difference between the relative timing of the dominant and opposite sign processes might create large changes in $\delta^{13}CO_2$. Amplitudes in $\delta^{13}CO_2$ caused by fast terrestrial uptake or release during millennial-scale climate variability depend not only on the amount of transferred carbon but also on the speed of these changes. Those which occur on timescales shorter than a millennium are not detectable in $\delta^{13}CO_2$ because of gas exchange equilibration with the surface ocean. The $\delta^{13}CO_2$ signal of fast processes, on the other hand, is largely attenuated in ice core records during the firnification and gas enclosure. We therefore suggest to measure $\delta^{13}CO_2$ with priority on ice cores with high temporal resolution and select times with rather fast climatic changes.

Citation: Köhler, P., H. Fischer, and J. Schmitt (2010), Atmospheric $\delta^{13}CO_2$ and its relation to pCO_2 and deep ocean $\delta^{13}C$ during the late Pleistocene, *Paleoceanography*, *25*, PA1213, doi:10.1029/2008PA001703.

1. Introduction

[2] Our understanding of the natural variability in the global carbon cycle is steadily increasing. Especially for the late Pleistocene both new data sets and model experiments were published recently. The atmospheric CO_2 record was now measured in ice cores over the last 800 kyr [*Petit et al.*, 1999; *Siegenthaler et al.*, 2005; *Lüthi et al.*, 2008]. A carbon cycle box model applied transiently in time gave some quantitative interpretation of glacial/interglacial (G/IG) changes in the carbon cycle over these times [*Köhler and Fischer*, 2006]. More complex approaches, such as Earth system models of intermediate complexity or ocean circulation models provide improved insight into the processes controlling atmospheric CO_2 in the past [e.g., *Brovkin et al.*, 2007; *Menviel et al.*, 2008a, 2008b; *Parekh et al.*, 2008; *Schmittner and Galbraith*, 2008; *Tschumi et al.*, 2008]. The interpretation of simulation results always depends on the accuracy by which processes are implemented in the models and, thus, a more complex understanding will emerge the more feedback processes are included. However, for the very long timescales of several glacial cycles we still have to rely on the faster and simpler approach of box models.

[3] A variable which could improve our interpretation capability of changes in the global carbon cycle is the ratio of stable carbon isotopes $\delta^{13}C$. It gives another boundary condition on temporal variability in the carbon cycle which has to be met by modeling experiments and could further constrain which processes are responsible for observed variations in atmospheric CO_2. Isotopic fractionation is associated with any biological, chemical, or physical process, thereby enriching/depleting ^{13}C relative to ^{12}C. In general, reaction rates involving the light isotope ^{12}C are greater than those involving the heavy isotope ^{13}C, thus leading to an enrichment of ^{13}C in the source, and to a depletion of ^{13}C in

[1]Alfred Wegener Institute for Polar and Marine Research, Bremerhaven, Germany.
[2]Climate and Environmental Physics, Physics Institute and Oeschger Centre for Climate Change Research, University of Bern, Bern, Switzerland.

0883-8305/10/2008PA001703

the sink of any exchange process [e.g., *Zeebe and Wolf-Gladrow*, 2001]. For example, terrestrial photosynthesis fractionates $\delta^{13}C$ by −5‰ to −27‰, depending on environmental conditions and photosynthetic pathway [*Lloyd and Farquhar*, 1994]. As a consequence, $\delta^{13}C$ values of the global vegetation are at present about 18‰ lower than $\delta^{13}CO_2$ of the atmosphere [*Scholze et al.*, 2003]. For the ocean/atmosphere system, the isotopic fractionation during air/sea gas exchange leads to $\delta^{13}C$ values of dissolved inorganic carbon (DIC) ($\delta^{13}C_{DIC}$) in the surface waters of 1.5‰ to 2‰ and to $\delta^{13}C$ of atmospheric CO_2 ($\delta^{13}CO_2$) which is about 8‰ lighter [*Kroopnick*, 1985; *Mook*, 1986; *Gruber et al.*, 1999]. Marine organisms use carbon from the DIC pool to built hard shells (calcification) and organic matter (photosynthesis). While photosynthesis at the ocean surface fractionates $\delta^{13}C$ by about −10‰ to −20‰ relative to CO_2 (aq) [*Goericke and Fry*, 1994], the incorporation of C in carbonate shells increases the $\delta^{13}C$ of the shells relative to HCO_3^- by about 2‰ [*Mook*, 1986]. Both organic carbon as well as carbonate shells are exported to the deep ocean, where most of them are remineralized or dissolved. This so-called biological pump establishes gradients with depth in both DIC and $\delta^{13}C_{DIC}$, which are counterbalanced by ocean circulation, bringing DIC rich waters, depleted in ^{13}C, back to the surface.

[4] The atmosphere exchanges carbon with both the land and the ocean, therefore atmospheric $\delta^{13}CO_2$ contains valuable information on the dynamics of both the marine and the terrestrial carbon cycle. Furthermore, $\delta^{13}CO_2$ can, as the atmospheric CO_2 concentration itself, in principle be measured directly in Antarctic ice cores. However, precise $\delta^{13}CO_2$ measurements on polar ice cores turned out to be one of the largest analytical challenges in paleoclimate research, the resolution and quality of the data sets to date are recently improved but they are still limited to the Holocene and the last G/IG transition [*Leuenberger et al.*, 1992; *Indermühle et al.*, 1999; *Smith et al.*, 1999; *Elsig et al.*, 2009; *Lourantou et al.*, 2010].

[5] Because measuring $\delta^{13}CO_2$ in ice core samples is a demanding and time consuming task it would help experimentalists to have an a priori estimate where large fluctuations in the $\delta^{13}CO_2$ record can be expected. This might help to constrain the temporal resolution desirable to capture the most important features of an ice core $\delta^{13}CO_2$ record. Accordingly we used the well tested BICYCLE model in this study in a similar setting as before [*Köhler and Fischer*, 2006] with the special focus on long-term changes in $\delta^{13}CO_2$ over the last 740 kyr. In order to test the model performance we compare the simulations in a first step briefly with atmospheric CO_2 as before, but more importantly with benthic $\delta^{13}C$ reconstructions from sediment cores from the deep Pacific, which are presumably a recorder of past variations on $\delta^{13}C_{DIC}$. The importance of different physical and biogeochemical processes, such as ocean circulation, marine export production, or terrestrial carbon storage, influencing all three variables (atmospheric CO_2 and $\delta^{13}CO_2$, deep Pacific $\delta^{13}C_{DIC}$) and the relationships between all of them will be discussed in detail. In addition, millennial-scale variability of the Dansgaard/Oeschger events and its effect on both terrestrial carbon storage and the marine carbon cycle are investigated in sensitivity studies.

2. Methods

2.1. BICYCLE: A Box Model of the Isotopic Carbon Cycle

[6] The box model of the global carbon cycle, BICYCLE, used in this study consists of ten homogeneously mixed ocean boxes distinguishing three vertical layers and three ocean basins (Figure 1), as well as a well mixed atmospheric box and a globally averaged terrestrial biosphere consisting of seven compartments with different photosynthetic pathways and soil turnover times. Prognostic variables are carbon (DIC in the ocean), $\delta^{13}C$ and $\Delta^{14}C$ in all boxes, and additionally alkalinity, PO_4 and O_2 in the ocean boxes. The model is based on former box models of the ocean and the terrestrial biosphere, but was adapted and updated in previous studies concentrating on Termination I. It is fully described by *Köhler and Fischer* [2004] (terrestrial part) and *Köhler et al.* [2005a] (marine part).

[7] In the terrestrial part, the values of six control parameters were derived in a sensitivity analysis to match literature targets of preindustrial and LGM vegetation and soil C contents, the fraction of C_4 vegetation and global net primary productivity (NPP). Out of about 10000 simulations two sets of parameter values with 12 and 14 ensemble members for the control functions meet our predefined targets. However, they differ in the way, how either CO_2 fertilization (TB_{CO_2}) or temperature changes ($TB_{\Delta T}$) dominate the dynamics of the terrestrial carbon storage over time. In our standard setup (scenario CTRL) we use a realization in which CO_2 fertilization is more important than temperature (TB_{CO_2}), which seems to be more in line with global dynamic vegetation models [e.g., *Joos et al.*, 2004], but the use of the more temperature dominated controls for terrestrial C storage ($TB_{\Delta T}$) will be used to analyze the potential impact of fast climate change.

[8] In the ocean, the $CaCO_3$, which enters the deep ocean boxes and can be accumulated in the sediments, was produced with a fixed C ratio between exported organic matter (OM) and hard shells in the surface waters (C_{OM}: C_{CaCO_3} = 10:1). C_{OM} export at 100 m depth is prescribed for present-day to 10 PgC [e.g., *Schlitzer*, 2000], but depends locally on available macronutrients, implying a global $CaCO_3$ export of 1 Pg C yr^{-1} similar to other applications [e.g., *Jin et al.*, 2006]. This is realized with maximum productivity (consumption of all PO_4) in the low-latitude surface boxes. Increased export might occur in the Southern Ocean, if macronutrients are available and the proxy for iron input into the Southern Ocean suggests the stimulation of additional productivity due to iron fertilization. $CaCO_3$ and C_{OM} are partially (20% and about 70%, respectively) dissolved or remineralized in the intermediate layers. In the deep ocean, carbonate compensation is calculated with a relaxation approach resulting in either sedimentation of $CaCO_3$ or dissolution of sediments as a function of offset from initial (present-day) CO_3^{2-} concentrations. The timescale of the sedimentary response (*e*-folding time τ of 1.5 kyr) was chosen to fit the measured relaxations of CO_3^{2-} anomalies in

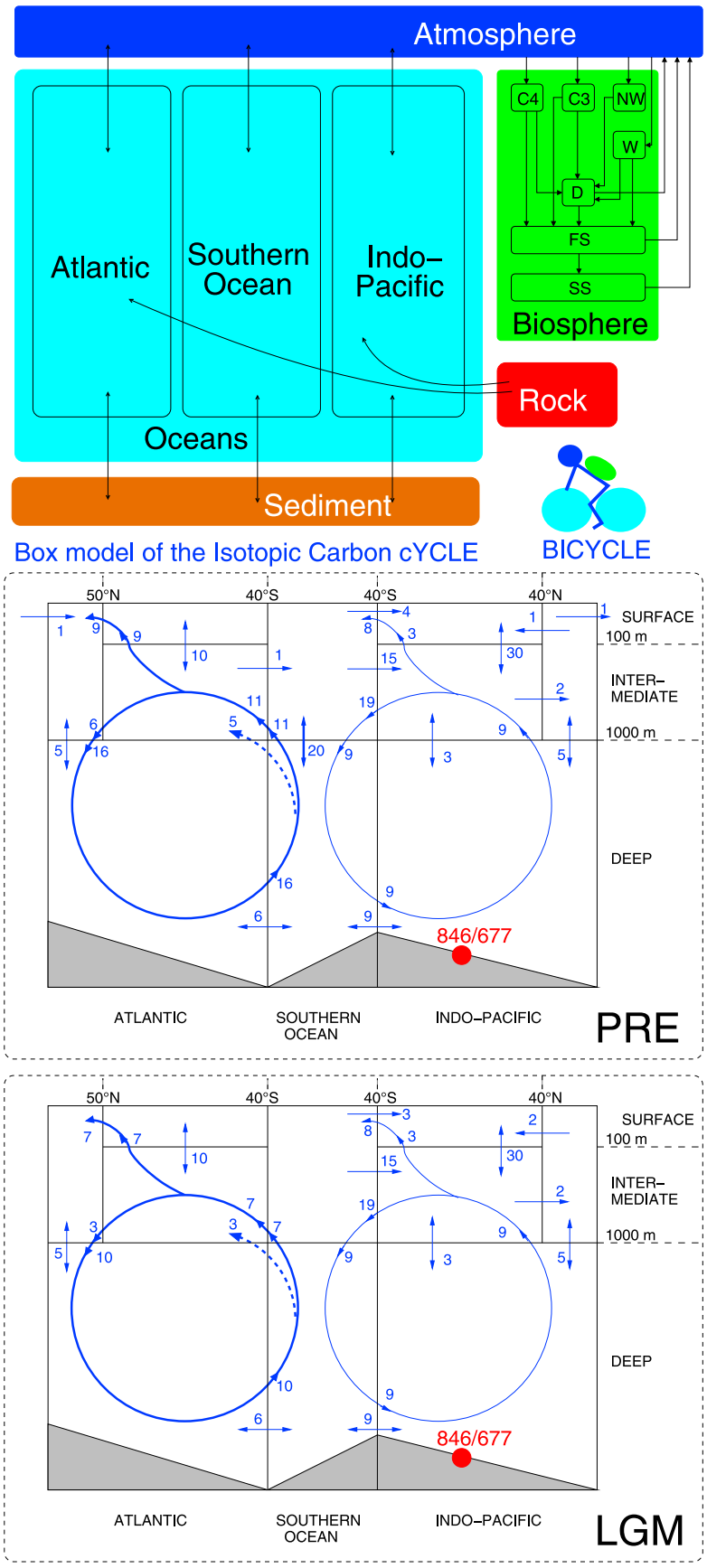
Atmosphere
Atlantic
Southern Ocean
Indo–Pacific
Oceans
Sediment
C4
C3
NW
W
D
FS
SS
Biosphere
Rock
Box model of the Isotopic Carbon cYCLE
BICYCLE
50°N
40°S
40°S
40°N
SURFACE
100 m
INTER–MEDIATE
1000 m
DEEP
846/677
ATLANTIC
SOUTHERN OCEAN
INDO–PACIFIC
PRE
LGM

Figure 1

the deep Pacific over the last 25 kyr [*Marchitto et al.*, 2005]. A larger τ, as suggested by some modeling studies [*Archer et al.*, 1997, 1998], would lead to longer delays in the carbonate compensation and thus to smaller glacial/interglacial amplitudes in atmospheric pCO_2 (see *Köhler and Fischer* [2006] for sensitivity studies on τ), but only to very little effects for the ^{13}C cycle. During sedimentation and dissolution no isotopic fractionation is assumed: $CaCO_3$ which is added to the sediments has the same $\delta^{13}C$ as during hard shell production at the water surface, while the dissolved sediments carry the $\delta^{13}C$ signal of the sediment box. Organic carbon in the sediments is not considered, thus, all C_{OM} reaching the deep ocean is remineralized. For the analysis of the ^{13}C cycle, a sediment box containing initially 50,000 Pg of inorganic carbon (as $CaCO_3$) is introduced in each deep ocean basin (Atlantic, Southern Ocean, Indo-Pacific). The initial $\delta^{13}C$ of the sediments (+2.75‰) is similar to the average signature of the $CaCO_3$ produced in the surface ocean. Initial values were chosen to minimize temporal drifts in $\delta^{13}C$ of the sediments.

[9] The present-day ocean circulation as depicted in Figure 1 was prescribed with results from the World Ocean Circulation Experiment (WOCE) [*Ganachaud and Wunsch*, 2000]. Assumed temporal changes in ocean circulation over time are (1) a reduced NADW formation (−40% during glacials) and subsequently slower Atlantic meridional overturning circulation (AMOC) [*Meissner et al.*, 2003]; however, we acknowledge that the precise state of the glacial circulation can still not be determined from the available proxy information [*Huybers et al.*, 2007; *Lynch-Stieglitz et al.*, 2007]; (2) a poorly ventilated glacial Southern Ocean (net vertical exchange at the LGM reduced to approximately a fourth of its preindustrial strength) deduced from $\delta^{13}C_{DIC}$ data [*Hodell et al.*, 2003]; and (3) a closure of the Bering Strait during sea level low stands (Figure 1).

[10] Three model improvements were performed since the first publication of BICYCLE: (1) carbonate compensation is now delayed by the *e*-folding time τ [*Köhler and Fischer*, 2006], while it was instantaneous before; (2) the introduction of sediment boxes, including $\delta^{13}C$ calculations, was necessary for longer simulation studies focusing on the ^{13}C cycle [*Köhler and Bintanja*, 2008]; and (3) ocean circulation was slightly revised [*Köhler and Bintanja*, 2008]. Previously, all of the upwelling water in the Southern Ocean was traveling through the Southern Ocean surface box. Now, 30% of the upwelling flux is immediately relocated to the intermediate box in the equatorial Atlantic (dashed lines in Figure 1). This is reasoned with the short residence time of these waters at the surface which is too short to equilibrate with the atmosphere. The revision has mainly implications for the simulated $\delta^{13}C_{DIC}$ in the intermediate and deep Atlantic ocean during the LGM (see section 2.3 for details).

[11] For the application presented here, BICYCLE was forced forward in time over the last 740 kyr by the use of various paleodata sets derived from ice and marine sediment cores. These proxy time series are used to prescribe temporal variations of climatic boundary conditions (sea level, sea ice coverage, ocean temperature, ocean circulation, marine export production, global mean temperature (affecting the terrestrial biosphere)). In that way, climate change is not internally calculated in our model, but prescribed externally implying a complete lack of carbon cycle-climate feedbacks in all our applications. A complete description of these data sets is found in the work by *Köhler and Fischer* [2006], in which the consequences of changing climate conditions on the carbon cycle and especially on atmospheric pCO_2 were analyzed. Here we use the same forcing data sets, but updated the time series derived from EPICA Dome C (δD, iron flux) to its new age scale EDC3 [*Parrenin et al.*, 2007].

2.2. Simulation Scenarios

[12] Additionally to the control simulation (CTRL) we performed some simulation scenarios to analyze the importance of fast climate changes on atmospheric $\delta^{13}CO_2$ in more detail (Table 1). These scenarios use atmospheric CH_4 concentration measured throughout the last 740 kyr in the EPICA Dome C ice core [*Loulergue et al.*, 2008] as crude proxy for Northern Hemispheric temperature change ($\Delta T_{NH}^{CH_4}$, important for the terrestrial C dynamics). This assumption is based on the synchroneity of fast changes in CH_4 and temperature proxies in Greenland ice cores throughout the last glacial cycle [*North Greenland Ice Core Project members*, 2004] and the strong increase in the atmospheric CH_4 north-south gradient during interstadials [*Dällenbach et al.*, 2000], that points to synchronous climate changes in northern boreal wetland regions. Accordingly, the approach to use CH_4 for ΔT_{NH} is more concentrating on the timing and abruptness of Dansgaard/Oeschger events while the absolute amplitude of concurrent Northern Hemisphere temperature is probably incorrect (Figure 2a). In the control simulation without rapid climate changes ΔT_{NH} was based on a model-based deconvolution of the LR04 benthic $\delta^{18}O$ stack (ΔT_{NH}^{LR04}) [*Bintanja et al.*, 2005; *Lisiecki and Raymo*, 2005] which has a temporal resolution of 1–2 kyr during the time window of interest. Therefore, by switching from LR04-$\delta^{18}O$ to CH_4 as forcing data set for ΔT_{NH} we are able to analyze the impact of climate changes faster than 1 kyr on the carbon cycle.

Figure 1. The BICYCLE carbon cycle model. (top) Main geometry. The terrestrial biosphere contains seven globally averaged reservoirs representing C_4 (turn over time τ = 4 years) and C_3 (τ = 5 years) grasses, nonwoody (NW) (τ = 2 years) and woody (W) (τ = 25 years) parts of trees, detritus (τ = 5 years), and fast (FS, τ = 100 years) and slow (SS, τ = 1000 years) decomposing soil. (middle and bottom) Geometry and ocean circulation fluxes (in Sv = 10^6 m^3 s^{-1}) of the oceanic module. PRE, preindustrial situation based on WOCE; LGM, assumed circulation during the LGM. The latitudinal position of the sediment cores (ODP677/846) used for comparison is indicated by the red dot. The conservation of water masses is checked and ensured for every time step. From *Köhler and Bintanja* [2008].

Table 1. Summary of Simulation Scenarios

Scenario	Characteristics	Forcing			
		TB[a]	ΔT_{NH}[b]	SST in NATL[c]	NADW[d]
S1.5K	Nearly identical to S1.5K of *Köhler and Fischer* [2006][e]	CO_2	LR04	ODP980	ODP980
CTRL	Identical to S1.5K in all aspects but with revised ocean circulation as plotted in Figure 1	CO_2	LR04	ODP980	ODP980
TB+	As CTRL, but temperature control of TB is prescribed with atmospheric CH_4 and ΔT becomes more important for C storage on land than CO_2 fertilization	ΔT	CH_4	ODP980	ODP980
TB+SST	As TB+, but changes in SST in North Atlantic were forced by CH_4	ΔT	CH_4	CH_4	ODP980
D/O	As TB+SST, but changes in NADW were forced by CH_4	ΔT	CH_4	CH_4	CH_4

[a]The parameterization of the forcing of the terrestrial biosphere (TB) follows either more CO_2 fertilization (CO_2) or more temperature changes (ΔT), corresponding to scenarios "case I" or "TB1" and "case I" or "TB2," respectively, in earlier publications [*Köhler and Fischer*, 2004; *Köhler et al.*, 2005a].
[b]ΔT_{NH} (used to force changes in terrestrial C storage) calculated either out of LR04 $\delta^{18}O$ [*Lisiecki and Raymo*, 2005] using an ice sheet–climate model [*Bintanja et al.*, 2005] or out of EPICA Dome C CH_4 [*Loulergue et al.*, 2008].
[c]SST in the North Atlantic is prescribed by ODP980 data [*McManus et al.*, 1999; *Wright and Flower*, 2002] or by the EPICA Dome C CH_4.
[d]Changes in NADW formation are prescribed by ODP980 data [*McManus et al.*, 1999; *Flower et al.*, 2000] or by the EPICA Dome C CH_4.
[e]The only change to scenario S1.5K of *Köhler and Fischer* [2006] is the update of the age model of the EPICA Dome C records.

[13] We proceed in three steps, introducing first CH_4 as proxy for ΔT_{NH} (scenario TB+). In this scenario the set of parameter values forcing the terrestrial part of the C cycle was switched to those depending more on Northern Hemispheric temperature than CO_2 ($TB_{\Delta T}$). This switch in the forcing was performed to constrain the potential range of variability to be recorded in $\delta^{13}CO_2$. In a second step (scenario TB+SST) $\Delta T_{NH}^{CH_4}$ is also taken to force SST changes in the North Atlantic surface box. In the third step (scenario D/O) those temperature changes were also used as prognostic driver of the strength of the NADW formation (Figure 2b). Consequently, the NADW formation is reduced from its interglacial strength (16 Sv) down to 2 Sv in scenario D/O, while it varies only between 10 and 16 Sv in all other simulations. Switching NADW formation between high interglacial and low glacial states in all but the D/O scenario is based on a threshold in benthic $\delta^{18}O$ in ODP980 in the North Atlantic [*Köhler and Fischer*, 2006]. The proposed strength of the NADW in the scenario D/O should explore the range of potential impacts on $\delta^{13}CO_2$ (including nearly complete shutdowns of the AMOC) but should not be understood as a suggestion how ocean circulation changed over time. The latter two scenarios (TB+SST, D/O) are designed to quantify the impact of fast climate changes on the marine carbon cycle. We understand these last scenarios as a zero-order case study, because the assumed changes in the SST and oceanic overturning are completely parameterized. Our approach is limited in various ways. For

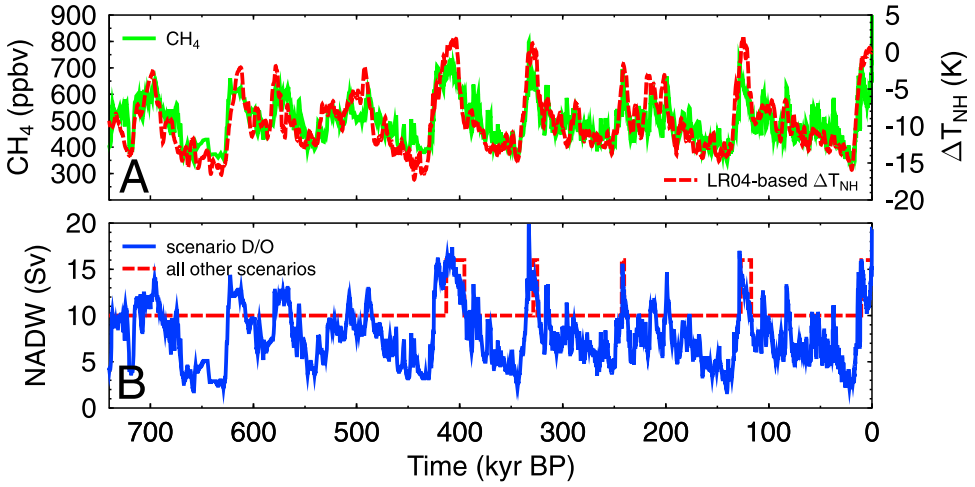

Figure 2. (a) Atmospheric CH_4 from EPICA Dome C [*Loulergue et al.*, 2008] and Northern Hemispheric temperature change ΔT_{NH} deconvolved from LR04 benthic $\delta^{18}O$ by ice sheet modeling [*Bintanja et al.*, 2005]. Both are used alternatively as proxy to force our simulation (see text and Table 1 for details). (b) Assumed changes in NADW formation and subsequent strength of the AMOC.

Table 2. Comparison of C Reservoirs and $\delta^{13}C$ Signature for Preindustrial and LGM Conditions for the Present Control Run and the Previous Run[a]

	Carbon					$\delta^{13}C$ (‰)			
	PRE			LGM		PRE		LGM	
	GLODAP	CTRL	GBC05	CTRL	GBC05	CTRL	GBC05	CTRL	GBC05
Ocean[b]									
Surface North Atlantic	2105	2111	2092	2133	2113	1.45	1.56	1.49	1.63
Surface equatorial Atlantic	2011	1987	1971	2065	2101	1.67	1.76	1.63	1.79
Surface Southern Ocean	2163	2152	2140	2188	2257	1.39	1.40	1.78	1.66
Surface equatorial Indo-Pacific	1963	1986	1976	2062	2109	1.38	1.42	1.57	1.56
Surface North Pacific	2252	2178	2167	2288	2339	1.52	1.57	1.51	1.45
Intermediate equatorial Atlantic	2143	2224	2177	2257	2207	0.49	0.76	**0.80**	**1.52**
Intermediate equatorial Indo-Pacific	2185	2202	2196	2263	2333	0.41	0.42	0.75	0.66
Deep Atlantic	2189	2233	2211	2347	2095	0.55	0.66	**0.18**	**0.81**
Deep Southern Ocean	2253	2250	2234	2549	2586	0.52	0.57	−0.64	−0.50
Deep Indo-Pacific	2317	2343	2332	2550	2603	0.08	0.10	−0.48	−0.44
Mean ocean	2249	2268	2253	2436	2438	0.39	0.44	−0.05	0.08
Atmosphere[c]		263	267	178	179	−6.61	−6.55	−6.60	−6.59

[a]For the preindustrial ocean DIC data from GLODAP (corrected for anthropogenic C) [*Key et al.*, 2004] are also shown. Note that the LGM in CTRL shows values for 21 kyr B.P. (time with pCO_2 minima), while the LGM in GBC05 shows those for 20 kyr B.P. (as published by *Köhler et al.* [2005a]). Bold numbers in $\delta^{13}C$ highlight the main differences and our reason for changing the circulation scheme. PRE, preindustrial; CTRL, present control run; GBC05, previous run [*Köhler et al.*, 2005a].

[b]Carbon as DIC (μmol kg^{-1}).

[c]Carbon as pCO_2 (μatm).

example, changes in SST have no influence on the circulation scheme, prescribed changes in ocean circulation are operating instantaneously without time delay and do not change ocean temperature. These details are better captured in general circulation models, which contain the respective physics of the ocean.

2.3. Model Validation

[14] We briefly evaluate here, how the model performance was modified as consequence of the three model improvements (Table 2). We therefore compare DIC and $\delta^{13}C_{DIC}$ of all oceanic reservoirs for the CTRL run and our previous application [*Köhler et al.*, 2005a, Tables 1 and 3] (labeled GBC05 hereafter) for preindustrial (PRE) and LGM climates. For the preindustrial ocean, DIC is furthermore compared with recent GLODAP measurements, which were corrected for anthropogenic C input [*Key et al.*, 2004].

[15] For the preindustrial situation, nearly all DIC values of GLODAP and our two simulations differ by less then 20 μmol kg^{-1}. Differences are only larger in the equatorial intermediate Atlantic (box 6, ~80 μmol kg^{-1}) and deep Atlantic (box 8, ~50 μmol kg^{-1}), which is probably the consequence of the revised overturning cell in the Atlantic ocean. The differences between CTRL and GBC05 at the LGM are between 20 and 70 μmol kg^{-1} for individual reservoirs, nearly negligible for the mean ocean, but about 350 μmol kg^{-1} in the deep Atlantic. Thus, the shortcut of upwelling waters via the intermediate box to the North Atlantic shifts the storage of C in the deep ocean slightly from the Indo-Pacific to the Atlantic. Even with these variabilities in DIC, atmospheric pCO_2 in both simulations is very similar for both climates (PRE, 263 versus 267 μatm and LGM, 178 versus 179 μatm).

[16] Differences in $\delta^{13}C_{DIC}$ are less than 0.1‰ (PRE) and 0.2‰ (LGM) in all boxes apart from the boxes 6 and 8. Here, $\delta^{13}C_{DIC}$ in CTRL is 0.3‰ (PRE) and 0.7‰ (LGM) lower in the intermediate Atlantic, and 0.1‰ (PRE) and 0.6‰ (LGM) in the deep Atlantic than in GBC05. These differences, especially in the LGM, were our motivation for the revision of the ocean circulation scheme. The DIC in GBC05 in the intermediate Atlantic has a $\delta^{13}C_{DIC}$ typical for surface, not for intermediate waters (~1.5‰), and with 0.8‰ the deep Atlantic was not in line with LGM reconstructions [*Curry and Oppo*, 2005]. However, we acknowledge that our box model by definition cannot resolve all major aspect of $\delta^{13}C_{DIC}$, e.g., vertical gradients within the Atlantic ocean.

[17] In summary, we believe that the refinements of the model performed over the years were necessary improvements to include processes relevant for long-term investigations of the ^{13}C cycle.

3. Results and Discussion

3.1. Simulated Deep Pacific $\delta^{13}C_{DIC}$ and the Sediment Record

[18] For a validation of our simulation results with paleodata sets we concentrate first on the well established records of $\delta^{13}C$ measured in benthic foraminifera derived from deep sea cores. Some benthic species are known to record a $\delta^{13}C$ signal which is offset from that of DIC in the surrounding waters by ~0.3‰–0.4‰ due to the phytodetritus or Mackensen effect [*Mackensen et al.*, 1993]. For the main paleoreconstructions of $\delta^{13}C$ used here the time series can be assumed to be unaffected by the phytodetritus effect (thus $\delta^{13}C = \delta^{13}C_{DIC}$) as discussed in detail elsewhere [*Raymo et al.*, 2004]. We focus only on changes in the deep Pacific Ocean as recorded in the sediment cores ODP677 (1°N, 84°W, 3461 m water depth [*Shackleton et al.*, 1990; *Raymo et al.*, 1997]) and ODP846 (3°S, 91°W, 3307 m water depth [*Mix et al.*, 1995a; *Raymo et al.*, 2004]). In the deep eastern Pacific, where our Pacific sites are located, the horizontal and vertical gradients in $\delta^{13}C_{DIC}$ in the modern ocean are

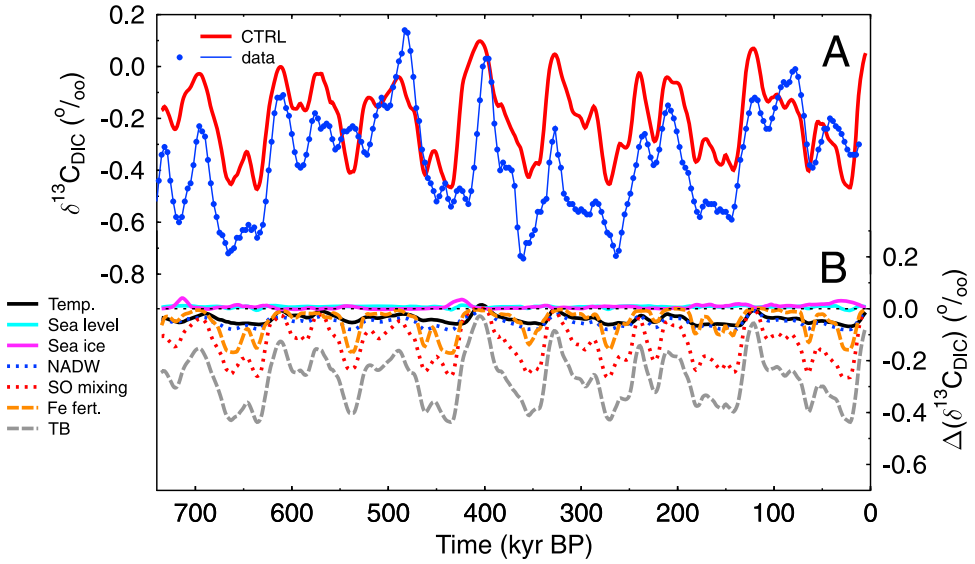

Figure 3. (a) Simulated $\delta^{13}C_{DIC}$ for the deep Indo-Pacific Ocean box for scenarios CTRL and data-based reconstruction. (b) Contribution of major processes to variations of deep Indo-Pacific $\delta^{13}C_{DIC}$: changes in ocean temperature (temp.), sea level, gas exchange through sea ice coverage (sea ice), strength of the NADW formation (NADW), Southern Ocean vertical mixing (SO mixing), iron fertilization in the Southern Ocean (Fe fert.), and carbon storage on land (TB). All simulation results are 9 kyr running means.

very small [*Kroopnick*, 1985]. A similar uniform distribution of $\delta^{13}C_{DIC}$ exists in large parts of the glacial Pacific [*Boyle*, 1992] (see also $\delta^{13}C_{DIC}$ data compilation in Figure 5 of *Köhler and Bintanja* [2008]). Therefore, observed changes are assumed to be representative of basin wide variations, which we can resolve with our coarse box model. The records are presented on the orbital tuned age scale derived for ODP677 by *Shackleton et al.* [1990]. They were interpolated to a uniform 3 kyr spacing and smoothed with a three-point running mean, as performed already in the compilation of *Raymo et al.* [2004]. For the comparison with our basin wide simulation results we will rely on the average of both sediment cores.

[19] Simulated $\delta^{13}C_{DIC}$ is smoothed with 9 kyr running mean to make it comparable with the benthic $\delta^{13}C_{DIC}$ reconstructions. Reconstructed deep Pacific $\delta^{13}C_{DIC}$ varies between +0.2‰ and −0.8‰. The data range (absolute maximum minus absolute minimum) in CTRL is with 0.7‰ somewhat smaller than the range (1.0‰) spanned by the data set (Figure 3a). This difference in absolute range is caused by the underlying 400 kyr cycle found in $\delta^{13}C_{DIC}$ reconstructions, which is (by definition) missing in the simulations, and which makes a point-to-point comparison of simulations and data impossible [*Mix et al.*, 1995b; *Wang et al.*, 2004; *Köhler and Bintanja*, 2008]. One hypothesis on its explanation is based on the variability of the hydrological cycle and weathering rates [*Wang*, 2007], which are both not included in our modeling approach and thus differences in this frequency domain between simulations and paleoreconstructions are expected. The general pattern on timescales up to 100 kyr (timing of strong changes in $\delta^{13}C_{DIC}$, G/IG amplitudes) is reproduced reasonably well in our simulations. The mean G/IG amplitudes in $\delta^{13}C_{DIC}$ over the last 740 kyr in CTRL and the reconstruction agree within their standard derivation (CTRL, 0.45‰ ± 0.11‰; data, 0.53‰ ± 0.07‰).

[20] The processes being mainly responsible for the simulated dynamics in deep Pacific $\delta^{13}C_{DIC}$ were identified by a factorial analysis (Figure 3b and Table 3). It is based on differences between CTRL and simulations in which the one process in question is shut off. Because $CaCO_3$ compensation is active in this factorial analysis the contributions of the individual processes include the partial effect of the sediment/ocean interaction. This factorial analysis is a first-order estimate of individual contributions which neglects nonlinear interacting effects. Terrestrial carbon storage is most important for low glacial deep ocean $\delta^{13}C_{DIC}$, because terrestrial carbon depleted in ^{13}C was released into the atmosphere during these times (−0.44‰ at the LGM). This is followed by Southern Ocean processes: (1) reduced vertical mixing (−0.26‰ at the LGM) leads to less glacial upwelling of DIC depleted in ^{13}C and an accumulation of isotopically light carbon in the abyss and (2) enhanced marine export production through iron fertilization (−0.16‰ at the LGM) brings more isotopically light carbon to the deep ocean. The contributions from sea ice, sea level, temperature and NADW formation strength (AMOC) to changes in deep Pacific $\delta^{13}C_{DIC}$ are very small (<±0.1‰ each throughout the last 740 kyr).

[21] In our control simulation the mean ocean $\delta^{13}C_{DIC}$ is 0.43‰ lower at the LGM than during preindustrial times (Table 3), which is slightly smaller than changes in the deep Pacific ocean (−0.47‰). This agrees within the uncertainties with data-based estimates of 0.32‰–0.46‰ [*Curry et al.*,

Table 3. Summary of the Contribution of Different Processes to the Simulated Changes in Atmospheric pCO_2 and $\delta^{13}CO_2$ and Deep Pacific $\delta^{13}C_{DIC}$ and Mean Ocean $\delta^{13}C_{DIC}$ During Termination I[a]

	Atmosphere $\Delta(\delta^{13}CO_2)$ (‰)	Atmosphere $\Delta(pCO_2)$ (μatm)	Deep Pacific $\Delta(\delta^{13}C_{DIC})$ (‰)	Mean Ocean $\Delta(\delta^{13}C_{DIC})$ (‰)
Process				
Lower ocean temperatures	−0.49	−30	−0.08	−0.07
Smaller terrestrial carbon storage	−0.44	+12	−0.44	−0.44
Lower sea level	+0.06	+14	−0.01	+0.02
Weaker NADW formation	+0.10	−24	−0.08	−0.08
Enhanced marine export production	+0.19	−28	−0.16	−0.10
Larger sea ice cover (gas exchange)	+0.18	+12	+0.03	+0.03
Higher Southern Ocean stratification	+0.31	−46	−0.26	−0.16
Summed-up changes	−0.09	−90	−1.00	−0.80
Simulated changes in CTRL	+0.00	−85	−0.47	−0.43
Nonlinearities[b]	−0.09	+5	+0.53	+0.40

[a]The contributions are calculated by subtracting results with the process in question switch off (all but one) from the control run.
[b]Nonlinearity values are sum minus CTRL.

1988; *Duplessy et al.*, 1988]. *Shackleton* [1977] was the first who proposed that the change in mean ocean $\delta^{13}C_{DIC}$ was caused by the injection of ^{13}C-depleted carbon from terrestrial pools and could be used to infer the magnitude of the changes in the land storage. *Bird et al.* [1994] used 0.32‰ as best guess for the rise in mean oceanic $\delta^{13}C_{DIC}$ from the LGM to present and calculated an increase in terrestrial carbon storage over Termination I of 250–650 PgC. To test this hypothesis independently we investigate if and how much other processes contribute to the changes in the mean ocean $\delta^{13}C_{DIC}$ by an additional simulation in which the terrestrial carbon pools were kept constant. Indeed, only about 10% of the G/IG changes in mean ocean $\delta^{13}C_{DIC}$ (0.035‰ in case of Termination I) are not of terrestrial origin, mainly caused by the changing C content of the atmosphere and the ocean.

[22] A comparison of our analysis for $\delta^{13}C_{DIC}$ with other simulation studies is restricted to *Brovkin et al.* [2007]. In all other glacial studies, which are available to us, no results for $\delta^{13}C_{DIC}$ are discussed, e.g., *Crucifix* [2005] analyzed only the effect of a changed ocean overturning on the distribution of carbon isotopes within the ocean. *Brovkin et al.* [2007] simulate a reduced terrestrial C storage of 540 PgC at the LGM responsible for a drop in mean ocean $\delta^{13}C_{DIC}$ of 0.4‰, in line with our results. In their study enhanced marine export production increases the vertical gradient in $\delta^{13}C_{DIC}$ by up to 0.2‰, while sea level change has no im-

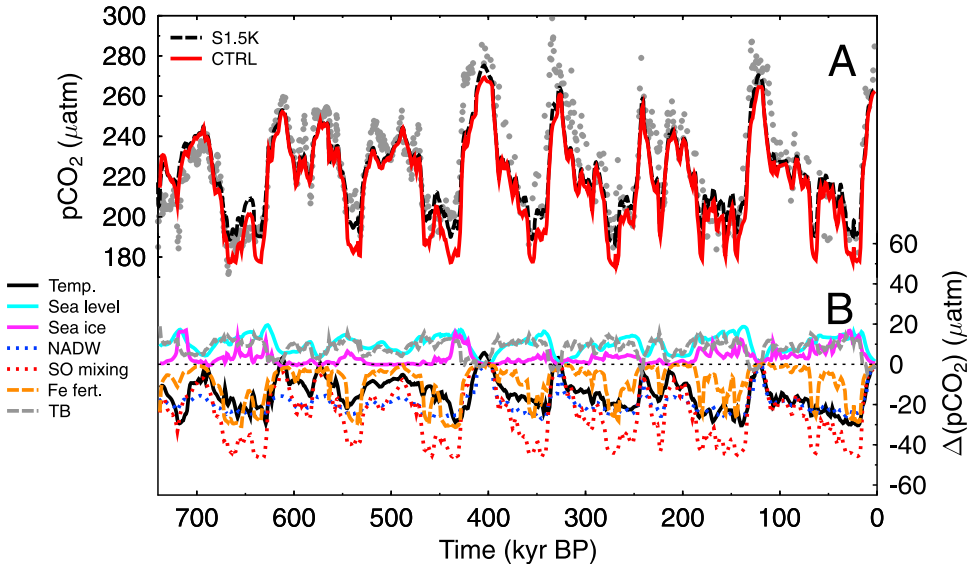

Figure 4. Simulated and measured atmospheric carbon dioxide. (a) Recent (CTRL (this study)) and previous (S1.5K [*Köhler and Fischer*, 2006]) control simulations. CO_2 data from Vostok [*Petit et al.*, 1999] on the orbitally tuned age scale [*Shackleton*, 2000] and EPICA Dome C data [*Siegenthaler et al.*, 2005; *Lüthi et al.*, 2008] on the gas age scale of the EDC3 dating [*Loulergue et al.*, 2007; *Parrenin et al.*, 2007]. (b) Contribution of major processes to variations in atmospheric pCO_2; see caption of Figure 3 for details.

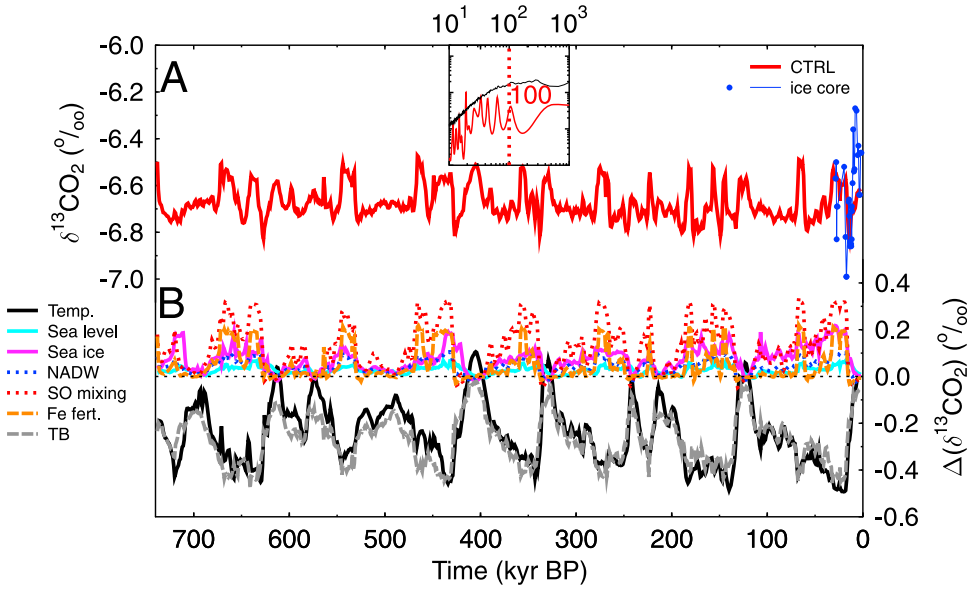

Figure 5. (a) Simulated atmospheric $\delta^{13}CO_2$ for scenarios CTRL and Taylor Dome $\delta^{13}CO_2$ ice core data [*Smith et al.*, 1999]. The inset shows maximum entropy spectral analysis (MESA) of $\delta^{13}CO_2$ in CTRL with black line showing the 99% confidence level. Labels on top of the plot show the length of the periods in years. (b) Contribution of major processes to variations in atmospheric $\delta^{13}CO_2$; see caption of Figure 3 for details.

pact on $\delta^{13}C_{DIC}$, which is again in line with our results (Table 3).

[23] In summary G/IG changes in deep Pacific $\delta^{13}C_{DIC}$ are reproduced in our model reasonably well, providing important constraints on the representativeness of our long-term terrestrial carbon cycle changes in our model and the uptake of additional carbon in the ocean.

3.2. Atmospheric pCO_2 and $\delta^{13}CO_2$ During the Last 740 kyr

[24] Both pCO_2 and $\delta^{13}CO_2$ time series are closely related to each other and understanding $\delta^{13}CO_2$ dynamics is not possible without investigations on pCO_2. Accordingly, we start with a short repetition of our simulation results for atmospheric pCO_2 to illustrate the representativeness of our model results compared to ice core measurements and to provide estimates of the influence of individual processes in the global carbon cycle in the past. An in-depth description of simulated and measured atmospheric carbon dioxide was previously published by *Köhler and Fischer* [2006].

[25] Simulated pCO_2 in CTRL varies between its glacial values of about 180 μatm and its maximum during interglacial of about 280 μatm. The simulated pCO_2 in CTRL during peak glacial times are about 10 μatm lower than in our previous model runs (scenario S1.5K of *Köhler and Fischer* [2006]) leading to 10 μatm larger G/IG amplitudes (Figure 4a), mainly related to the change in the Southern Ocean hydrography in our model. This glacial offset counterbalances the effect of a time delayed carbonate compensation (which reduces G/IG amplitudes in pCO_2). Our results here are therefore for Termination I very similar to those published by *Köhler et al.* [2005a].

[26] In CTRL, atmospheric $\delta^{13}CO_2$ is very similar during glacial maxima and the following full interglacial (Figure 5a). However, during the transition from a glacial to an interglacial state $\delta^{13}CO_2$ drops by 0.2‰ to 0.3‰ before it regains previous values. These dynamics of minimum $\delta^{13}CO_2$ for intermediate pCO_2 values are clearly illustrated in a scatterplot (Figure 6a) and fit to the general behavior seen in the ice core data from Taylor Dome [*Smith et al.*, 1999], however, the range of $\delta^{13}CO_2$ is about twice as large in the measurements than in the simulations for scenario CTRL.

[27] Throughout the last 740 kyr simulated atmospheric $\delta^{13}CO_2$ (Figure 5a) fluctuates with subglacial frequency between −6.8‰ and −6.5‰ (CTRL). In a spectral analysis (inset in Figure 5a) no significant components with periods around 100 kyr are found, which is remarkable, because this frequency is found in most paleoclimatic records of the late Pleistocene [*Hays et al.*, 1976], including atmospheric CO_2 (and even deep Pacific $\delta^{13}C_{DIC}$) and in the records which force BICYCLE forward in time.

[28] A factorial analysis equivalent to that shown for benthic $\delta^{13}C_{DIC}$ above was performed to identify which processes contribute to the changes in atmospheric pCO_2 and $\delta^{13}CO_2$ (Figures 4b and 5b and Table 3) in our model.

[29] 1. The process being most important for lowering glacial atmospheric $\delta^{13}CO_2$ is the ocean temperature leading to a reduction at the LGM of −0.49‰. Ocean temperature is one process, which influences $\delta^{13}CO_2$ and pCO_2 in a similar manner: reduced temperatures lead to a high oceanic carbon uptake (atmospheric pCO_2, −30 μatm at the LGM), preferable of the heavier isotope, thus depleting $\delta^{13}CO_2$ and reducing pCO_2 at the same time.

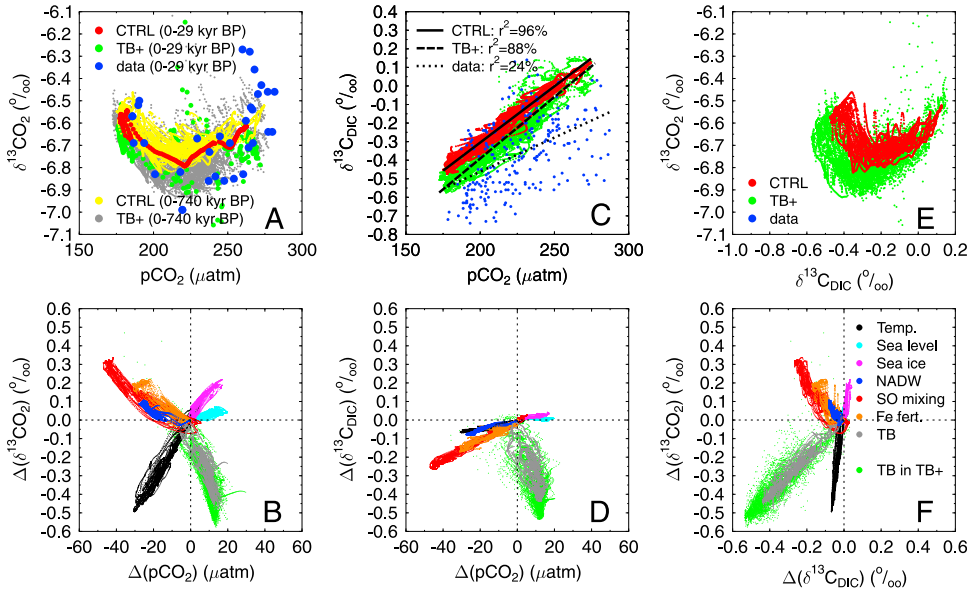

Figure 6. (a) Scatterplot of atmospheric pCO_2 and $\delta^{13}CO_2$ of simulations and data from the Taylor Dome ice core data over the last 29 kyr. (b) Contribution of individual processes in a similar scatterplot to Figure 6a over the whole simulation period. (c) Scatterplot of atmospheric pCO_2 and deep Pacific $\delta^{13}C_{DIC}$ of simulations and sediment data over the whole simulation period. (d) Contribution of individual processes in a similar scatterplot to Figure 6c. (e) Scatterplot of deep Pacific $\delta^{13}C_{DIC}$ and atmospheric $\delta^{13}CO_2$ of simulations over the whole simulation period. (f) Contribution of individual processes in a similar scatterplot to Figure 6d. See caption of Figure 3 for details on the different processes. The legend in Figure 6e is also valid for Figure 6c, and that in Figure 6f is also valid for Figures 6b and 6d.

[30] 2. Second most important for the dynamic of $\delta^{13}CO_2$ is the terrestrial carbon storage. The release of about 500 PgC of ^{13}C-depleted terrestrial carbon (with $\delta^{13}C$ between −20‰ and −25‰) results in a drop in $\delta^{13}CO_2$ by 0.44‰ in the LGM and a rise in pCO_2 by only 12 μatm.

[31] 3. Changes in sea level are nearly neutral for $\delta^{13}CO_2$. Its small effect of +0.06‰ for the LGM is connected with the 3% higher salinity, which leads to an outgassing and a rise of pCO_2 by 14 μatm.

[32] 4. Within BICYCLE an ocean with a weaker AMOC stores more carbon ($\Delta pCO_2 = -24$ μatm at the LGM). This results from the balance of carbon uptake in the region of the NADW formation and carbon release in the Southern Ocean, where the circulation of the AMOC comes back to the surface [*Mikaloff-Fletcher et al.*, 2007]. The effect of the AMOC on $\delta^{13}CO_2$ is an increase at the LGM of +0.10‰ caused by less upwelling of carbon-enriched deep waters (depleted in $\delta^{13}C_{DIC}$) in the Southern Ocean.

[33] 5. An enhanced glacial marine export production, stimulated by additional aeolian iron input into the Southern Ocean, leads to a rise in $\delta^{13}CO_2$ by +0.19‰ and a drop in pCO_2 by 28 μatm at the LGM. Export of organic matter rises from present 10.0 Pg C yr^{-1} to 12.5 Pg C yr^{-1} at the LGM. Organic carbon is depleted in ^{13}C (e.g., $\delta^{13}C$ between −20‰ and −30‰ [*Goericke and Fry*, 1994]); consequently DIC of the surface waters becomes enriched in ^{13}C and so CO_2 of the atmosphere.

[34] 6. A larger sea ice cover at the LGM reduces the gas exchange. It was shown [*Köhler and Fischer*, 2006] that sea ice in the north and in the south has opposing effects on atmospheric CO_2 because they block the gas exchange in either a sink region (north) or a source region (south) for atmospheric CO_2 [*Mikaloff-Fletcher et al.*, 2007]. It was furthermore analyzed, that in the present model configuration the gas exchange effects of sea ice in the north dominate in our model over that in the south resulting in a pCO_2 rise of 12 μatm at the LGM. Accordingly, larger glacial sea ice reduces the oceanic carbon uptake. As mentioned earlier, the isotopic fractionation during gas exchange is temperature-dependent with preferential uptake of ^{13}C during cold temperatures. A reduction of the gas exchange at the cold high latitudes implies less gas exchange during cold conditions and therefore less uptake of ^{13}C, leading consequently to a rise in $\delta^{13}CO_2$ of +0.18‰ during the LGM.

[35] 7. The process having the largest positive impact on glacial $\delta^{13}CO_2$ (+0.31‰ at the LGM) and at the same time the largest negative impact on pCO_2 (−46 μatm at the LGM) is the stratification in the Southern Ocean. The underlying principles are the same as for a reduced AMOC: less vertical exchange during glacials brings less deep waters enriched in DIC and depleted in ^{13}C to the surface. Consequently, the DIC of the surface waters become progressively enriched in ^{13}C (i.e., increasing the vertical gradient in $\delta^{13}C_{DIC}$ in the ocean), thus increasing also atmospheric $\delta^{13}CO_2$ via gas exchange.

[36] Altogether, the dynamics in the simulated atmospheric pCO_2 and $\delta^{13}CO_2$ can be understood in the context of our modeling exercise. Marine processes, mainly those

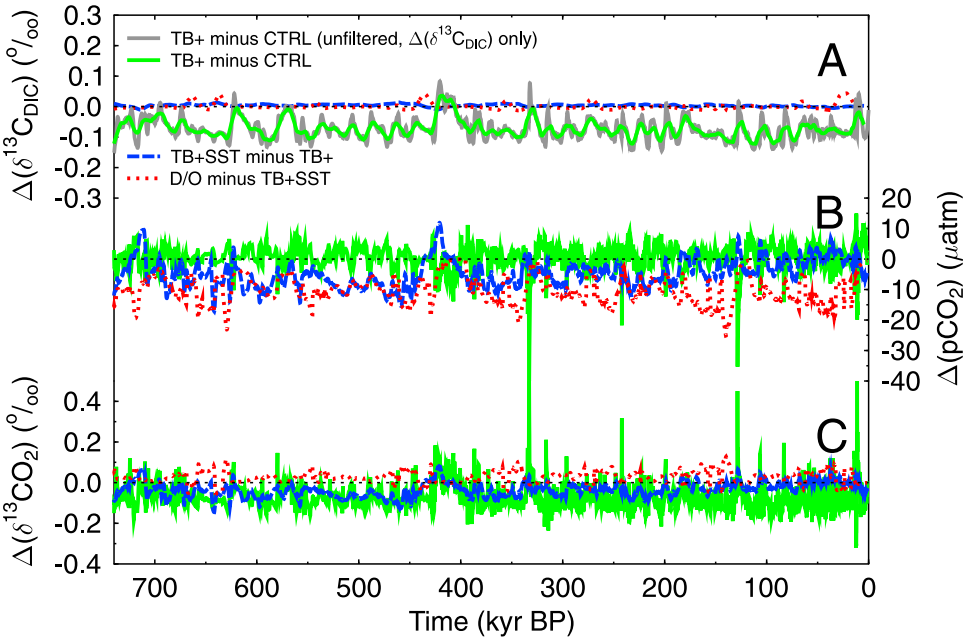

Figure 7. Additional contributions of fast climate change scenarios. See Table 1 for details. (a) The $\delta^{13}C_{DIC}$ of the deep Indo-Pacific. (b) Atmospheric pCO_2. (c) Atmospheric $\delta^{13}CO_2$. All simulation results in Figure 7a (apart from the unfiltered one) are 9 kyr running means; in Figures 7b and 7c unfiltered data are shown.

responsible for the depth gradient in $\delta^{13}C_{DIC}$ in the water column (biological pump and ocean circulation) compensate the effects of temperature and terrestrial light carbon on atmospheric $\delta^{13}CO_2$, consequently leading to a lack in 100 kyr periodicity.

3.3. Relationships Between Atmospheric pCO_2, $\delta^{13}CO_2$, and Deep Pacific $\delta^{13}C_{DIC}$

[37] If we now analyze in detail, which processes are controlling atmospheric pCO_2, $\delta^{13}CO_2$ and deep Pacific $\delta^{13}C_{DIC}$ at the same time some interesting conclusions can be drawn (Table 3). Apart from sea ice coverage (with sea level being neutral), all processes lead to a lower glacial $\delta^{13}C_{DIC}$ in the deep ocean. Hence, deep ocean $\delta^{13}C_{DIC}$ in effect integrates constructively the process operating over the G/IG cycles. This very much contrasts with the atmosphere, for which $\delta^{13}CO_2$ is dominated by four (if one includes sea ice) processes with comparable magnitudes of impact, but differing in sign (two negative, two positive). Thus, no clearly expressed G/IG variations in $\delta^{13}CO_2$ are expected. However, any large excursions in $\delta^{13}CO_2$ (in either direction) are not only possible, but a priori expected, as any small phase difference between the relative timing of the dominant and oppositely sign processes may create short-lived, transient changes in $\delta^{13}CO_2$. Note that some of these transient changes in Figure 5 may be due to real phase differences in carbon cycle changes, while others may be artifacts caused by an imperfect synchroneity of the timescales of the individual proxy records used to force BICYCLE forward in time.

[38] Apart from the terrestrial C storage all processes influence in-phase pCO_2 and $\delta^{13}C_{DIC}$, meaning they either increase or decrease both at the same time. If plotted pairwise together in a scatterplot (Figure 6c) deep Pacific $\delta^{13}C_{DIC}$ and atmospheric pCO_2 are in the modeling world strongly coupled and linearly related (r^2 = 96% for CTRL). Thus, deep Pacific $\delta^{13}C_{DIC}$ has the potential to be used as a predictor for pCO_2 for times without ice core measurements. However, in reality (if ice core CO_2 and benthic $\delta^{13}C_{DIC}$ are plotted against other) their relationship is blurred (r^2 = 24%), mainly because of the underlying 400 kyr cycle in benthic $\delta^{13}C_{DIC}$, but probably also due to a mismatch of the individual age scales.

3.4. Fast Climate Changes

[39] In our model atmospheric pCO_2 fluctuates on millennial timescales with amplitudes smaller than 10 μatm if fast climate changes and fast changes in terrestrial carbon storage (scenario TB+) are simulated (Figure 7). Only for very few events peak amplitudes in pCO_2 are up to 35 μatm. Assuming furthermore also fast changes in the marine carbon cycle (scenarios TB+SST and D/O) shifts the simulated pCO_2 throughout the simulation period to lower values. In scenario D/O this is caused by the on average slower AMOC.

[40] In scenario TB+ the data range in the scatterplot of $\delta^{13}CO_2$ and pCO_2 is extended to values as low as −7.1‰, similar to the measurements in the Taylor Dome ice core (Figure 6a). A point-to-point comparison of simulated and measured data over Termination I is of limited value, as assumed changes in our scenarios were not chosen to optimize any fit to the Taylor Dome data. We admit that for the present study a poor fit of the simulations and the measurements over Termination I exists, because we did not

implement in our time-dependent forcing all abrupt climate changes in detail, but we were interested in the principle behavior of the system. However, the relative dating of different forcing factors (e.g., warming in the north and the south) is important to be able to compare simulated $\delta^{13}CO_2$ with measurements. This misfit is based on the design of our simulations scenarios, was expected and has therefore no consequences for our general conclusions. For more details on Termination I, please see *Köhler et al.* [2005a] and *Lourantou et al.* [2010]. There, it is shown that the w shape pattern of $\delta^{13}CO_2$ between 20 and 10 kyr B.P. might have been caused by an initial decrease in $\delta^{13}CO_2$ caused by the resumed Southern Ocean ventilation and reduced marine export production, which is followed by variability mainly caused by terrestrial C uptake and release during the Bølling/Allerød–Younger Dryas–Early Holocene climate variability.

[41] Large amplitudes in $\delta^{13}CO_2$ on the order of 0.5‰ occur at 333, 129 and 11 kyr B.P. (Figure 7c). A consideration of fast climate changes in the ocean (scenarios TB +SST and D/O) leads only to small additional changes in $\delta^{13}CO_2$ (<0.1‰). Furthermore, the effects of both processes nearly compensate each other (Figure 7c).

[42] Simulated deep Pacific $\delta^{13}C_{DIC}$ is only very weakly (<0.05‰) affected by fast changes in the marine carbon cycle (scenarios TB+SST and D/O) (Figure 7a). However, if the land uptake and release of C is fast (TB+) an additional variability of the order of 0.1‰ is introduced. This additional variability between TB+ and CTRL is due the chosen parameter set in TB+ which favors C_4 over C_3 grasses during the LGM and which then leads to a higher $\delta^{13}C$ value of the terrestrial biosphere in TB+ than in CTRL and as consequence to lower oceanic $\delta^{13}C_{DIC}$ values.

[43] How can we understand the importance of fast terrestrial C uptake/release on $\delta^{13}CO_2$? According to the concept of the bipolar seesaw [*Stocker and Johnsen*, 2003] the AMOC is reorganized during Dansgaard/Oeschger climate fluctuations [*Johnsen et al.*, 1992; *EPICA Community Members*, 2006]. If the AMOC weakens, temperatures in the North Atlantic region and over large parts of the northern continents drop by 5–20 K [*Lang et al.*, 1999; *Knutti et al.*, 2004]. In a study with the LPJ state-of-the-art vegetation model [*Köhler et al.*, 2005b] the tree line in the northern high latitudes shifts southward during these cold temperatures and isotopic light terrestrial carbon is released to the atmosphere. Furthermore, peak-to-peak amplitudes in atmospheric $\delta^{13}CO_2$ caused by land carbon release of up to 150 PgC during AMOC weakening were as big as −0.25%.

[44] In the results presented here, the contribution of the marine carbon cycle to fast variability in $\delta^{13}CO_2$ is rather small. We like to stress that our model may have deficiencies in appropriately simulating the overall response of the marine carbon cycle to fast climate changes because of missing ecological processes and coarse spatial resolution. Other studies with more complex models find much larger changes in the marine export production during millennial-scale climate variability [*Schmittner*, 2005; *Menviel et al.*, 2008a; *Schmittner and Galbraith*, 2008]. The most recent study by *Menviel et al.* [2008a], which uses the LOVECLIM model, simulates a 130 PgC release from land during an AMOC shutdown and the time delayed C uptake of 100 PgC in the ocean resulting in a +20 μatm peak in pCO_2. Both findings are in line with our simulation results: more C is stored in the ocean with a slowing of the AMOC, and less C is stored on land. However, the consequences of fast AMOC variability or Dansgaard/Oeschger events for atmospheric $\delta^{13}CO_2$ are so far not covered in the other studies and can therefore not be compared here.

[45] A transient simulation with the Bern2.5D model was mimicking the Younger Dryas (YD) cold event by an AMOC shutdown [*Marchal et al.*, 1998]. In that model the AMOC shutdown (with constant terrestrial C storage) led to a rise in $\delta^{13}C_{DIC}$ in North Atlantic surface waters by 1.5‰ (changes in atmospheric $\delta^{13}CO_2$ were not shown), partially caused by both reduced overturning and smaller marine export production.

[46] In a model intercomparison study on carbon cycle–climate feedbacks for the 21st century all but one of the eleven models exhibited stronger sensitivities to climate warming for land C storage than for ocean C storage [*Friedlingstein et al.*, 2006]. Under the assumption that future warming is a specific case of fast climate change, these stronger terrestrial sensitivities are in line with our findings.

3.5. Timescales of Carbon Exchange Processes

[47] With some additional simulations we investigated the influence of the speed of fast climate change (stadials to interstadials and vice versa) on the carbon cycle (Figure 8). Terrestrial carbon uptake of 150 PgC over 100 years is followed by a stable period of 1 kyr and then by a gradual release of 150 PgC over 100 and more (up to 5000) years. The initial $\delta^{13}CO_2$ peak of +0.62‰ caused by the terrestrial uptake of isotopically light carbon is reduced to less than a fifth (+0.11‰) after only 200 years. For the following C release the amplitudes vary from −0.62‰ (100 years) over −0.21‰ (500 years) and −0.14‰ (1000 years) to zero (5000 years). The effect is small to nondetectable in slow climate transitions. Attenuation is less important for pCO_2 than for $\delta^{13}CO_2$ because the pCO_2 amplitudes depend on net ocean uptake which is buffered by the carbonate system (for details see *Zeebe and Wolf-Gladrow* [2001]), while for $\delta^{13}CO_2$ the amplitude is reduced by the much faster air-sea gas exchange with the surface ocean.

[48] In addition to this timescale dependency inherent to the carbon exchange processes between ocean and atmosphere, gas samples in ice cores contain (due to the continuous bubble close-off process in the firn) air with a certain age distribution rather than a single age. This gas age distribution is a function of local conditions at the ice core site and is calculated with firnification models [*Schwander et al.*, 1993; *Spahni et al.*, 2003]. For EPICA Dome C it can be approximated with a lognormal function (Figure 9):

$$y = \frac{1}{x \cdot \sigma \cdot \sqrt{2\pi}} \cdot e^{-0.5\left(\frac{\ln(x)-\mu}{\sigma}\right)^2}, \quad (1)$$

with gas age x in years. We chose for simplicity $\sigma = 1$, which leads to an expected mean gas age of $E = e^{\mu-0.5}$. With $E_{PRE} = 213$ years and $E_{LGM} = 590$ years given by the model

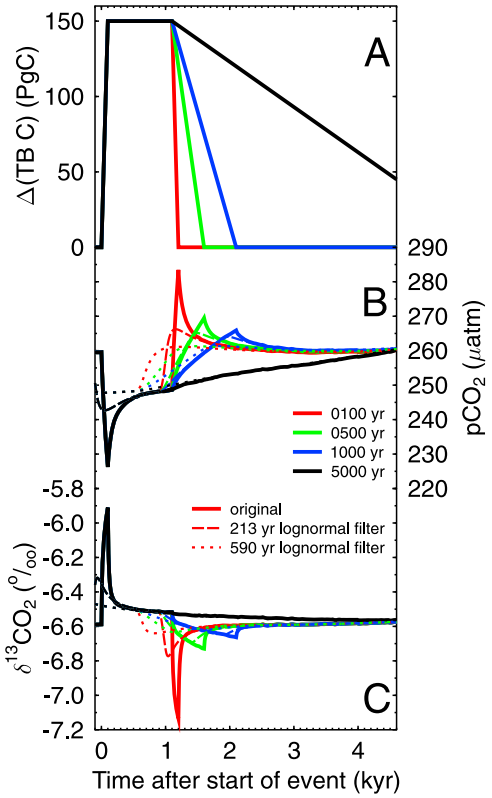

Figure 8. (a) Simulation of terrestrial carbon uptake of 150 PgC in 100 years, followed after 1 kyr by the release of 150 PgC within 100, 500, 1000, and 5000 years and effects on (b) atmospheric pCO_2 and (c) $\delta^{13}CO_2$. The terrestrial biosphere fractionates $\delta^{13}C$ during carbon uptake by 16‰, typical for LGM conditions [*Scholze et al.*, 2003; *Köhler and Fischer*, 2004]. Solid lines represent original results. Dashed and dotted lines represent after filtering with a lognormal function with mean gas age distribution of 213 years (PRE) and 590 years (LGM), respectively, to mimic amplitude attenuation during gas enclose in the ice core.

of *Joos and Spahni* [2008] our analytic function is fully described and can be used as filter to calculate how the original atmospheric signal is attenuated by the firnification processes and which signals might be recorded in an ice core with climatic conditions typical for EPICA Dome C. These gas age distributions for LGM and preindustrial climates can be considered as extremes with the gas distributions for other climate in between.

[49] The filtering of the atmospheric signals by the gas age distribution reduces the original atmospheric amplitude in pCO_2 for the fastest event (35 μatm in 100 years) to 51% (PRE) and 37% (LGM) in the ice core. The attenuation of the amplitude is even larger for atmospheric $\delta^{13}CO_2$, because of the faster signal dampening via air-sea gas exchange. The 0.62‰ peak during the fast climate transition (100 years) is reduced to 42% (PRE) or 21% (LGM). Furthermore, due to lognormal distribution of the gas age the peak maximum is shifted in time toward earlier years, e.g., up to 350 years in $\delta^{13}CO_2$ for LGM climate conditions. This shift in the time of the peak maxima is implicitly included in the gas age scales developed for ice cores.

[50] These two effects on $\delta^{13}CO_2$ taken together, signal dilution of slow and attenuation of fast events, poses a conflict of interest for the observer which is difficult to overcome. Fast events produce the largest amplitudes in $\delta^{13}CO_2$, but their original sizes are difficult to determine, while signals of slow events vanish quickly due the gas exchange with the ocean. In order to gain the most information from ice core $\delta^{13}CO_2$ records we therefore suggest to first concentrate on fast climate transitions, following several steps: (1) identify climate transitions in CH_4 which are fast (<one century) at both the onset and the end, (2) use those ice cores for $\delta^{13}CO_2$ measurements with highest temporal resolution (thus snow accumulation) available, and (3) to compare carbon cycle modeling results with $\delta^{13}CO_2$ measurements one needs to account for the temporal smoothing during the firnification process. This can be achieved by filtering of simulated atmospheric $\delta^{13}CO_2$ with an assumed gas age distribution as done here.

[51] For the comparison of simulation results and measurements it is so far not clear how fast the carbon cycle is responding to rapid climate change. Models so far suggest that the carbon cycle responds to an AMOC shutdown within several centuries [*Köhler et al.*, 2005b; *Menviel et al.*, 2008a]. However, these models simulate also temperature anomalies, which are slower than data-based evidences of climate switches within less than a decade [*Steffensen et al.*, 2008]. Recently, one modeling study generated for the first time temperature anomalies over central Greenland on the order and abruptness found in ice core [*Smith and Gregory*, 2009]. They found, that their model behavior critically depends on the region in which freshwater was put into the North Atlantic in order to generate the climate anomalies. *Clement and Peterson* [2008] analyzed three different mechanisms potentially causing abrupt climate change

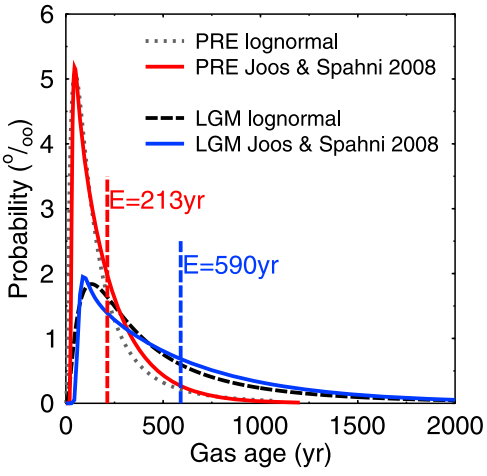

Figure 9. Gas age distribution as function of climate state for preindustrial (PRE) and LGM conditions. Calculation by *Joos and Spahni* [2008], approximated by lognormal functions.

(ocean circulation, sea ice feedbacks, tropical processes) and found that each of these mechanisms has explanatory strengths and weaknesses. If the conclusions of these studies are included in future carbon cycle–climate studies, we can expect to generate fast climate changes, which are in better agreement with the reconstructions.

4. Conclusions

[52] We analyzed the individual contributions of processes changing atmospheric pCO_2 and $\delta^{13}CO_2$ as well as deep Pacific $\delta^{13}C_{DIC}$ in the carbon cycle box model BICYCLE throughout the last 740 kyr. The different dynamics (in terms of response to G/IG changes) in atmospheric $\delta^{13}CO_2$ in comparison to both atmospheric CO_2 and deep Pacific $\delta^{13}C_{DIC}$ are consistent with our understanding for each of the underlying processes. Only a 400 kyr variability in deep Pacific $\delta^{13}C_{DIC}$, that potentially points to a long-term weathering feedback, is not included in our model runs. Our analyses clearly show that mean ocean and deep Pacific $\delta^{13}C_{DIC}$ are mainly controlled by the G/IG terrestrial C uptake and release. In contrast, pCO_2 and $\delta^{13}CO_2$ changes represent mainly a mixture of ocean-related processes superimposed on the slow G/IG change in terrestrial carbon storage. Atmospheric pCO_2 and deep Pacific $\delta^{13}C_{DIC}$ are in principle related to each other and if the latter is high-pass filtered to suppress the 1/400 kyr^{-1} frequencies, $\delta^{13}C_{DIC}$ has the potential to predict the variability in atmospheric pCO_2 in times without ice core measurements.

[53] When changing all individual processes at the same time the different effects on atmospheric $\delta^{13}CO_2$ largely compensate each other and cancel all variability with frequencies of 1/100 kyr^{-1} in atmospheric $\delta^{13}CO_2$. Large excursions in $\delta^{13}CO_2$ on shorter timescales can occur, as any small phase difference between the relative timing of the dominant and oppositely sign processes might create large changes in $\delta^{13}CO_2$. Amplitudes in $\delta^{13}CO_2$ caused by fast terrestrial uptake or release may be imprinted in $\delta^{13}CO_2$ but depend not only on the amount of transferred carbon, but also on the speed of these changes. Those, which occur on timescales slower than a millennium are leaving only a subtle imprint in $\delta^{13}CO_2$. The consequence is that typical stadial/interstadial transitions (abrupt warming in the Northern Hemisphere in less than a century) leave a distinct signal in $\delta^{13}CO_2$, while the reverse cooling causes only a subtle reverse trend.

[54] The proposed high-frequency variability in atmospheric $\delta^{13}CO_2$ together with signal dilution of slower events and amplitude attenuation of fast events due to the gas age distribution in ice cores calls for both a high temporal resolution and a high precision of atmospheric $\delta^{13}CO_2$ in ice core analysis. A filtering of simulated atmospheric $\delta^{13}CO_2$ with the assumed gas age distribution as done here is necessary for events faster than one century to correct for the temporal smoothing due to the firnification process before ice core measurements and carbon cycle simulations become comparable. Despite those complications, it is the strength of atmospheric $\delta^{13}CO_2$ that it allows us to critically evaluate model results and our general understanding of the global carbon cycle since a large set of processes have to be well captured at the right timing within the models.

[55] **Acknowledgments.** We thank Andy Ridgwell and André Paul for their constructive reviews. Renato Spahni kindly provided us with his modeling results on the gas age distribution of CO_2. Funding for this work has come in part from the German climate research program DEKLIM.

References

Archer, D., H. Kheshgi, and E. Maier-Reimer (1997), Multiple timescales for neutralization of fossil fuel CO_2, *Geophys. Res. Lett.*, *24*, 405–408.

Archer, D., H. Kheshgi, and E. Maier-Reimer (1998), Dynamics of fossil fuel neutralization by marine $CaCO_3$, *Global Biogeochem. Cycles*, *12*, 259–276.

Bintanja, R., R. van de Wal, and J. Oerlemans (2005), Modelled atmospheric temperatures and global sea levels over the past million years, *Nature*, *437*, 125–128, doi:10.1038/nature03975.

Bird, M. I., J. Lloyd, and G. D. Farquhar (1994), Terrestrial carbon storage at the LGM, *Nature*, *371*, 566.

Boyle, E. A. (1992), Cadmium and $\delta^{13}C$ paleochemical ocean distributions during the stage 2 glacial maximum, *Annu. Rev. Earth Planet. Sci.*, *20*, 245–287.

Brovkin, V., A. Ganopolski, D. Archer, and S. Rahmstorf (2007), Lowering of glacial atmospheric CO_2 in response to changes in oceanic circulation and marine biogeochemistry, *Paleoceanography*, *22*, PA4202, doi:10.1029/2006PA001380.

Clement, A. C., and L. C. Peterson (2008), Mechanisms of abrupt climate change of the last glacial period, *Rev. Geophys.*, *46*, RG4002, doi:10.1029/2006RG000204.

Crucifix, M. (2005), Distribution of carbon isotopes in the glacial ocean: A model study, *Paleoceanography*, *20*, PA4020, doi:10.1029/2005PA001131.

Curry, W. B., and D. W. Oppo (2005), Glacial water mass geometry and the distribution of $\delta^{13}C$ of ΣCO_2 in the western Atlantic Ocean, *Paleoceanography*, *20*, PA1017, doi:10.1029/2004PA001021.

Curry, W. B., J. C. Duplessy, L. D. Labeyrie, and N. J. Shackleton (1988), Changes in the distribution of $\delta^{13}C$ of deep water ΣCO_2 between the last glaciation and the Holocene, *Paleoceanography*, *3*, 317–341.

Dällenbach, A., B. Blunier, J. Flückiger, B. Stauffer, J. Chappellaz, and D. Raynaud (2000), Changes in the atmospheric CH_4 gradient between Greenland and Antarctica during the last glacial and the transition to the Holocene, *Geophys. Res. Lett.*, *27*, 1005–1008.

Duplessy, J. C., N. J. Shackleton, R. G. Fairbanks, L. Labeyrie, D. Oppo, and N. Kallel (1988), Deep water source variations during the last climatic cycle and their impact on the global deepwater circulation, *Paleoceanography*, *3*, 343–360.

Elsig, J., J. Schmitt, D. Leuenberger, R. Schneider, M. Eyer, M. Leuenberger, F. Joos, H. Fischer, and T. F. Stocker (2009), Stable isotope constraints on Holocene carbon cycle changes from an Antarctic ice core, *Nature*, *461*, 507–510, doi:10.1038/nature08393.

EPICA Community Members (2006), One-to-one coupling of glacial climate variability in Greenland and Antarctica, *Nature*, *444*, 195–198, doi:10.1038/nature05301.

Flower, B. P., D. W. Oppo, J. F. McManus, K. A. Venz, D. A. Hodell, and J. L. Cullen (2000), North Atlantic intermediate to deep water circulation and chemical stratification during the past 1 Myr, *Paleoceanography*, *15*, 388–403.

Friedlingstein, P., et al. (2006), Climate–carbon cycle feedback analysis: Results from the C^4MIP model intercomparison, *J. Clim.*, *19*, 3337–3353, doi:10.1175/JCLI3800.1.

Ganachaud, A., and C. Wunsch (2000), Improved estimates of global ocean circulation, heat transport and mixing from hydrographic data, *Nature*, *408*, 453–457.

Goericke, R., and B. Fry (1994), Variations of marine plankton $\delta^{13}C$ with latitude, temperature, and dissolved CO_2 in the world ocean, *Global Biogeochem. Cycles*, *8*, 85–90.

Gruber, N., C. D. Keeling, R. B. Bacastow, P. R. Guenther, T. J. Luecker, M. Wahlen, H. A. J. Meijer, W. G. Mook, and T. F. Stocker (1999), Spatiotemporal patterns of carbon-13 in the global surface oceans and the oceanic Suess effect, *Global Biogeochem. Cycles*, *13*, 307–335.

Hays, J. D., J. Imbrie, and N. J. Shackelton (1976), Variations in the Earth's orbit: Pacemaker of the ice ages, *Science*, *194*, 1121–1132.

Hodell, D. A., K. A. Venz, C. D. Charles, and U. S. Ninnemann (2003), Pleistocene vertical carbon isotope and carbonate gradients in the South Atlantic sector of the Southern Ocean, *Geochem. Geophys. Geosyst.*, *4*(1), 1004, doi:10.1029/2002GC000367.

Huybers, P., G. Gebbie, and O. Marchal (2007), Can paleoceanographic tracers constrain meridional circulation rates?, *J. Phys. Oceanogr.*, *37*, 394–407, doi:10.1175/JPO3018.1.

Indermühle, A., et al. (1999), Holocene carbon-cycle dynamics based on CO_2 trapped in ice at Taylor dome, Antarctica, *Nature*, *398*, 121–126.

Jin, X., N. Gruber, J. P. Dunne, J. L. Sarmiento, and R. A. Armstrong (2006), Diagnosing the contribution of phytoplankton functional groups to the production and export of particulate organic carbon, $CaCO_3$, and opal from global nutrient and alkalinity distributions, *Global Biogeochem. Cycles*, *20*, GB2015, doi:10.1029/2005GB002532.

Johnsen, S. J., H. B. Clausen, W. Dansgaard, K. Fuhrer, N. Gundestrup, C. U. Hammer, P. Iversen, J. Jouzel, B. Stauffer, and J. P. Steffensen (1992), Irregular glacial interstadials recorded in a new Greenland ice core, *Nature*, *359*, 311–313.

Joos, F., and R. Spahni (2008), Rates of change in natural and anthropogenic radiative forcing over the past 20,000 years, *Proc. Natl. Acad. Sci. U. S. A.*, *105*, 1425–1430, doi:10.1073/pnas.0707386105.

Joos, F., S. Gerber, I. C. Prentice, B. L. Otto-Bliesner, and P. J. Valdes (2004), Transient simulations of Holocenic atmospheric carbon dioxide and terrestrial carbon since the Last Glacial Maximum, *Global Biogeochem. Cycles*, *18*, GB2002, doi:10.1029/2003GB002156.

Key, R. M., A. Kozyr, C. L. Sabine, K. Lee, R. Wanninkhof, J. L. Bullister, R. A. Feely, F. J. Millero, C. Mordy, and T.-H. Peng (2004), A global ocean carbon climatology: Results from Global Data Analysis Project (GLODAP), *Global Biogeochem. Cycles*, *18*, GB4031, doi:10.1029/2004GB002247.

Knutti, R., J. Flückiger, T. F. Stocker, and A. Timmermann (2004), Strong hemispheric coupling of glacial climate through continental freshwater discharge and ocean circulation, *Nature*, *430*, 851–856.

Köhler, P., and R. Bintanja (2008), The carbon cycle during the mid Pleistocene transition: The Southern Ocean decoupling hypothesis, *Clim. Past*, *4*, 311–332.

Köhler, P., and H. Fischer (2004), Simulating changes in the terrestrial biosphere during the last glacial/interglacial transition, *Global Planet. Change*, *43*, 33–55, doi:10.1016/j.gloplacha.2004.02.005.

Köhler, P., and H. Fischer (2006), Simulating low frequency changes in atmospheric CO_2 during the last 740 000 years, *Clim. Past*, *2*, 57–78.

Köhler, P., H. Fischer, G. Munhoven, and R. E. Zeebe (2005a), Quantitative interpretation of atmospheric carbon records over the last glacial termination, *Global Biogeochem. Cycles*, *19*, GB4020, doi:10.1029/2004GB002345.

Köhler, P., F. Joos, S. Gerber, and R. Knutti (2005b), Simulated changes in vegetation distribution, land carbon storage, and atmospheric CO_2 in response to a collapse of the North Atlantic thermohaline circulation, *Clim. Dyn.*, *25*, 689–708, doi:10.1007/s00382-005-0058-8.

Kroopnick, P. M. (1985), The distribution of ^{13}C of ΣCO_2 in the world oceans, *Deep Sea Res., Part A*, *32*, 57–84.

Lang, C., M. Leuenberger, J. Schwander, and S. Johnsen (1999), 16°C rapid temperature variation in central Greenland 70,000 years ago, *Science*, *286*, 934–937.

Leuenberger, M., U. Siegenthaler, and C. C. Langway (1992), Carbon isotope composition of atmospheric CO_2 during the last ice age from an Antarctic ice core, *Nature*, *357*, 488–490.

Lisiecki, L. E., and M. E. Raymo (2005), A Pliocene-Pleistocene stack of 57 globally distributed benthic $\delta^{18}O$ records, *Paleoceanography*, *20*, PA1003, doi:10.1029/2004PA001071.

Lloyd, J., and G. D. Farquhar (1994), ^{13}C discrimination during CO_2 assimilation by the terrestrial biosphere, *Oecologia*, *99*, 201–215.

Loulergue, L., F. Parrenin, T. Blunier, J.-M. Barnola, R. Spahni, A. Schilt, G. Raisbeck, and J. Chappellaz (2007), New constraints on the gas age–ice age difference along the EPICA ice cores, 0–50 kyr, *Clim. Past*, *3*, 527–540.

Loulergue, L., A. Schilt, R. Spahni, V. Masson-Delmotte, T. Blunier, B. Lemieux, J.-M. Barnola, D. Raynaud, T. F. Stocker, and J. Chappellaz (2008), Orbital and millennial-scale features of atmospheric CH_4 over the past 800,000 years, *Nature*, *453*, 383–386, doi:10.1038/nature06950.

Lourantou, A., J. V. Lavrič, P. Köhler, J.-M. Barnola, D. Paillard, E. Michel, D. Raynaud, and J. Chappellaz (2010), New atmospheric carbon isotopic measurements constrain the CO_2 rise during the last deglaciation, *Global Biogeochem. Cycles*, doi:10.1029/2009GB003545, in press.

Lüthi, D., et al. (2008), High-resolution CO_2 concentration record 650,000–800,000 years before present, *Nature*, *453*, 379–382, doi:10.1038/nature06949.

Lynch-Stieglitz, J., et al. (2007), Atlantic meridional overturning circulation during the Last Glacial Maximum, *Science*, *316*, 66–69, doi:10.1126/science.1137127.

Mackensen, A., H.-W. Hubberten, T. Bickert, G. Fischer, and D. K. Fütterer (1993), The $\delta^{13}C$ in benthic foraminiferal tests of *Fontbotia wuellerstorfi* (Schwager) relative to the $\delta^{13}C$ of dissolved inorganic carbon in Southern Ocean deep water: Implications for glacial ocean circulation models, *Paleoceanography*, *8*, 587–610.

Marchal, O., T. F. Stocker, and F. Joos (1998), Impact of oceanic reorganizations on the ocean carbon cycle and atmospheric carbon dioxide content, *Paleoceanography*, *13*, 225–244.

Marchitto, T. M., J. Lynch-Stieglitz, and S. R. Hemming (2005), Deep Pacific $CaCO_3$ compensation and glacial-interglacial atmospheric CO_2, *Earth Planet. Sci. Lett.*, *231*, 317–336.

McManus, J. F., D. W. Oppo, and J. L. Cullen (1999), A 0.5-million-year record of millennial-scale climate variability in the North Atlantic, *Science*, *283*, 971–975.

Meissner, K. J., A. Schmittner, A. J. Weaver, and J. F. Adkins (2003), Ventilation of the North Atlantic Ocean during the Last Glacial Maximum: A comparison between simulated and observed radiocarbon ages, *Paleoceanography*, *18*(2), 1023, doi:10.1029/2002PA000762.

Menviel, L., A. Timmermann, A. Mouchet, and O. Timm (2008a), Meridional reorganization of marine and terrestrial productivity during Heinrich events, *Paleoceanography*, *23*, PA1203, doi:10.1029/2007PA001445.

Menviel, L., A. Timmermann, A. Mouchet, and O. Timm (2008b), Climate and marine carbon cycle response to changes in the strength of the Southern Hemispheric westerlies, *Paleoceanography*, *23*, PA4201, doi:10.1029/2008PA001604.

Mikaloff Fletcher, S. E., et al. (2007), Inverse estimate of the oceanic sources and sinks of natural CO_2 and the implied oceanic carbon transport, *Global Biogeochem. Cycles*, *21*, GB1010, doi:10.1029/2006GB002751.

Mix, A. C., J. Le, and N. J. Shackleton (1995a), Benthic foraminiferal stable isotope stratigraphy of Site 846: 0–1.8 Ma, *Proc. Ocean Drill. Program Sci. Results*, *138*, 839–854.

Mix, A. C., N. G. Pisias, W. Rugh, J. Wilson, A. Morey, and T. K. Hagelberg (1995b), Benthic foraminiferal stable isotope record from Site 849 (0–5 Ma): Local and global climate changes, *Proc. Ocean Drill. Program Sci. Results*, *138*, 371–412.

Mook, W. G. (1986), ^{13}C in atmospheric CO_2, *Neth. J. Sea Res.*, *20*(2–3), 211–223.

North Greenland Ice Core Project members (2004), High-resolution record of Northern Hemisphere climate extending into the last interglacial period, *Nature*, *431*, 147–151.

Parekh, P., F. Joos, and S. A. Müller (2008), A modeling assessment of the interplay between aeolian iron fluxes and iron-binding ligands in controlling carbon dioxide fluctuations during Antarctic warm events, *Paleoceanography*, *23*, PA4202, doi:10.1029/2007PA001531.

Parrenin, F., et al. (2007), The EDC3 chronology for the EPICA Dome C ice core, *Clim. Past*, *3*, 485–497.

Petit, J. R., et al. (1999), Climate and atmospheric history of the past 420,000 years from the Vostok ice core, Antarctica, *Nature*, *399*, 429–436.

Raymo, M. E., D. W. Oppo, and W. Curry (1997), The mid-Pleistocene climate transition: A deep sea carbon isotopic perspective, *Paleoceanography*, *12*, 546–559.

Raymo, M. E., D. W. Oppo, B. P. Flower, D. A. Hodell, J. F. McManus, K. A. Venz, K. F. Kleiven, and K. McIntyre (2004), Stability of North Atlantic water masses in face of pronounced climate variability during the Pleistocene, *Paleoceanography*, *19*, PA2008, doi:10.1029/2003PA000921.

Schlitzer, R. (2000), Applying the adjoint method for biogeochemical modeling: Export of particulate organic matter in the world ocean, in *Inverse Methods in Global Biogeochemical Cycles*, *Geophys. Monogr. Ser.*, vol. 114, edited by P. Kasibhatla et al., pp. 107–124, AGU, Washington, D. C.

Schmittner, A. (2005), Decline of the marine ecosystem caused by a reduction in the Atlantic overturning circulation, *Nature*, *434*, 628–633.

Schmittner, A., and E. D. Galbraith (2008), Glacial greenhouse-gas fluctuations controlled by ocean circulation changes, *Nature*, *456*, 373–376, doi:10.1038/nature07531.

Scholze, M., J. O. Kaplan, W. Knorr, and M. Heimann (2003), Climate and interannual variability of the atmosphere-biosphere $^{13}CO_2$ flux, *Geophys. Res. Lett.*, *30*(2), 1097, doi:10.1029/2002GL015631.

Schwander, J., J.-M. Barnola, C. Andrié, M. Leuenberger, A. Ludin, D. Raynaud, and B. Stauffer (1993), The age of the air in the firn and the ice at Summit, Greenland, *J. Geophys. Res.*, *98*, 2831–2838.

Shackleton, N. J. (1977), Carbon 13 in Uvigerina: Tropical rainforest history and the equatorial Pacific carbonate dissolution cycles, in *The Fate of Fossil Fuel CO_2 in the Oceans*, edited by N. R. Anderson and A. Malahoff, pp. 401–427, Plenum, New York.

Shackleton, N. J. (2000), The 100,000-year ice-age cycle identified and found to lag temperature, carbon dioxide, and orbital eccentricity, *Science*, *289*, 1897–1902.

Shackleton, N. J., A. Berger, and W. P. Peltier (1990), An alternative astronomical calibration of the lower Pleistocene timescale based on OPD Site 677, *Trans. R. Soc. Edinburgh Earth Sci.*, *81*, 251–261.

Siegenthaler, U., et al. (2005), Stable carbon cycle–climate relationship during the late Pleistocene, *Science*, *310*, 1313–1317, doi:10.1126/science.1120130.

Smith, H. J., H. Fischer, M. Wahlen, D. Mastroianni, and B. Deck (1999), Dual modes of the carbon cycle since the Last Glacial Maximum, *Nature*, *400*, 248–250.

Smith, R. S., and J. M. Gregory (2009), A study of the sensitivity of ocean overturning circulation and climate to freshwater input in different regions of the North Atlantic, *Geophys. Res. Lett.*, *36*, L15701, doi:10.1029/2009GL038607.

Spahni, R., J. Schwander, J. Flückiger, B. Stauffer, J. Chappellaz, and D. Raynaud (2003), The attenuation of fast atmospheric CH_4 variations recorded in polar ice cores, *Geophys. Res. Lett.*, *30*(11), 1571, doi:10.1029/2003GL017093.

Steffensen, J. P., et al. (2008), High-resolution Greenland ice core data show abrupt climate change happens in few years, *Science*, *321*, 680–684, doi:10.1126/science.1157707.

Stocker, T. F., and S. J. Johnsen (2003), A minimum thermodynamic model for the bipolar seesaw, *Paleoceanography*, *18*(4), 1087, doi:10.1029/2003PA000920.

Tschumi, T., F. Joos, and P. Parekh (2008), How important are Southern Hemisphere wind changes for low glacial carbon dioxide? A model study, *Paleoceanography*, *23*, PA4208, doi:10.1029/2008PA001592.

Wang, P. X. (2007), Feeling the Earth's pulse from global monsoon records, *Geophys. Res. Abstr.*, *9*, 05820, sref:1607-7962/gra/EGU2007-A-05820.

Wang, P., J. Tian, X. Cheng, C. Liu, and J. Xu (2004), Major Pleistocene stages in a carbon perspective: The South China Sea record and its global comparison, *Paleoceanography*, *19*, PA4005, doi:10.1029/2003PA000991.

Wright, A. K., and B. P. Flower (2002), Surface and deep ocean circulation in the subpolar North Atlantic during the mid-Pleistocene revolution, *Paleoceanography*, *17*(4), 1068, doi:10.1029/2002PA000782.

Zeebe, R. E., and D. A. Wolf-Gladrow (2001), *CO_2 in Seawater: Equilibrium, Kinetics, Isotopes*, *Elsevier Oceanogr. Ser.*, *65*, 346 pp.

H. Fischer and J. Schmitt, Climate and Environmental Physics, Physics Institute, University of Bern, Sidlerstr. 5, CH-3012 Bern, Switzerland. (hubertus.fischer@climate.unibe.ch; schmitt@climate.unibe.ch)

P. Köhler, Alfred Wegener Institute for Polar and Marine Research, PO Box 120161, D-27515 Bremerhaven, Germany. (peter.koehler@awi.de)